

NOTE

A surgical device for radiofrequency ablation of large liver tumors

I dos Santos¹, D Correia¹, A J M Soares¹, J A Góes¹, A F da Rocha¹,
D Schutt² and D Haemmerich^{2,3}

¹ Department of Electrical Engineering, University of Brasilia, Brasilia, DF 70910-900, Brazil

² Division of Pediatric Cardiology, Medical University of South Carolina, 165 Ashley Ave.,
Charleston, SC 29425, USA

³ Department of Bioengineering, Clemson University, Clemson, SC 29634, USA

E-mail: haemmer@musc.edu

Received 7 July 2008, accepted for publication 5 August 2008

Published 23 September 2008

Online at stacks.iop.org/PM/29/N59

Abstract

Radiofrequency ablation has become an accepted treatment option of patients with primary and metastatic liver tumors. We propose an ablation electrode array consisting of 4–8 blade shaped electrodes arranged in a circular geometry for the treatment of large liver tumors. We developed a 3D code based on the finite difference method for evaluating the effect of different numbers of electrodes (4, 6 and 8) and electrode distance on lesion size. The configuration with six electrodes can ablate a volume of $70 \times 70 \times 40 \text{ mm}^3$ in approximately 5 min, with tissue temperature above $50 \text{ }^\circ\text{C}$ throughout the treatment volume. We then performed an experimental study in polyacrylamide gel in order to validate the theoretical results. The average temperature error between the simulation and the experiment was 3.8% at the center of the electrode array. This study shows that the proposed device potentially allows more rapid treatment of large tumors than current radiofrequency ablation devices.

Keywords: liver, tumor, radiofrequency ablation, electrodes, finite difference method

1. Introduction

Radiofrequency (RF) ablation is an accepted, heat-based method used for treating cancer of the liver, kidney, bone and lung in certain patient populations (Ni *et al* 2005, Gillams 2005, Nguyen *et al* 2005, Mayo-Smith and Dupuy 2004, Gervais *et al* 2003, Groenemeyer *et al* 2002, Curley *et al* 2002, Neeman and Wood 2002). During RF ablation, electrodes are inserted percutaneously (i.e. through a small incision), during laparoscopy, or during surgery

and RF energy is applied through the electrodes. The tumor is destroyed by coagulation necrosis once it reaches temperatures higher than 50 °C for approximately 1–3 min. A current limitation of the RF tumor ablation is the inability of prevailing devices to treat tumors larger than 5 cm. Previous studies have proposed a new method of rapidly switching RF energy between multiple electrodes (Schutt *et al* 2008, Haemmerich *et al* 2004, Lee *et al* 2003), which allows the use of multiple RF electrodes simultaneously, reducing the treatment time.

RF ablation is usually performed by heating the entire volume of the tumor by placing an electrode in the tumor, and the tumor is heated from the inside out. A single ablation with current devices takes between 12 and 35 min and creates an ablation zone of 3–4 cm in diameter, depending on the device type. For large tumors, multiple ablations have to be performed sequentially (Dodd *et al* 2001). This method is both technically difficult and time consuming. This work presents a new approach where multiple electrodes are placed surrounding the tumor, allowing rapid heating of the tumor volume in a single ablation procedure. Furthermore, unlike conventional ablation devices, there is no need for ground pads, which eliminates the risk of skin burns below the pads. Figure 1(a) shows the electrode arrangement for a six-electrode configuration. In our design, multiple electrodes are placed circumferentially around the tumor. Thus, different from previous RF ablation devices, the tumor is heated from the outside, i.e., the temperature propagates from the electrodes to the center of the array. RF energy is applied in bipolar mode between opposing electrodes, and switched in short (0.1 s) intervals between electrode pairs (see figure 1(b)). Since tissue heating is a comparably slow process with time constants in the second range, all electrodes effectively heat the tissue simultaneously. The number of electrodes as well as their dimensions determines the total volume to be isolated.

In this work, the new electrode configuration is computationally analyzed and experimentally validated. A code based on the finite-difference method (FDM) was developed. The FDM has some advantages over the finite-element method (FEM) if the structure does not have a complex geometry and can be based on a regular mesh. This method is matrix-free and is usually faster than the FEM for the same mesh size. The FDM was used for all the derivatives involved in the equations.

The objective of the proposed ablation device was to achieve a faster ablation of large tumors than current devices. In this work, we investigated three different electrode configurations. Arrays of four, six and eight electrodes were simulated. In order to determine the coagulation zone, we investigated the behavior of the proposed configurations with respect to the radial distance between the opposite electrodes and with respect to the applied voltage. Moreover, we built an experimental device prototype in order to validate the numerical results.

2. Materials and methods

2.1. Numerical model

In order to simulate the structure shown in figure 1(b), we used the finite difference method (FDM) based on Pennes' bioheat equation (Pennes 1948):

$$\rho c \frac{\partial T}{\partial t} = \nabla \cdot (k \nabla T) + \mathbf{J} \cdot \mathbf{E} - \rho_b c_b \omega (T - T_b) \quad (1)$$

where T is the temperature (K), \mathbf{J} is the current density (A m^{-2}), \mathbf{E} is the electric field intensity (V m^{-1}), ρ is the density (kg m^{-3}), c is the specific heat ($\text{J kg}^{-1} \text{K}^{-1}$), k is the heat conduction coefficient ($\text{W m}^{-1} \text{K}^{-1}$), ρ_b is the blood density (kg m^{-3}), c_b is the specific heat of the blood ($\text{J kg}^{-1} \text{K}^{-1}$), ω is the blood perfusion coefficient (s^{-1}) and T_b is the blood temperature (K). Equation (1) defines the solution in the spatial domain including both the electrodes and tissue.

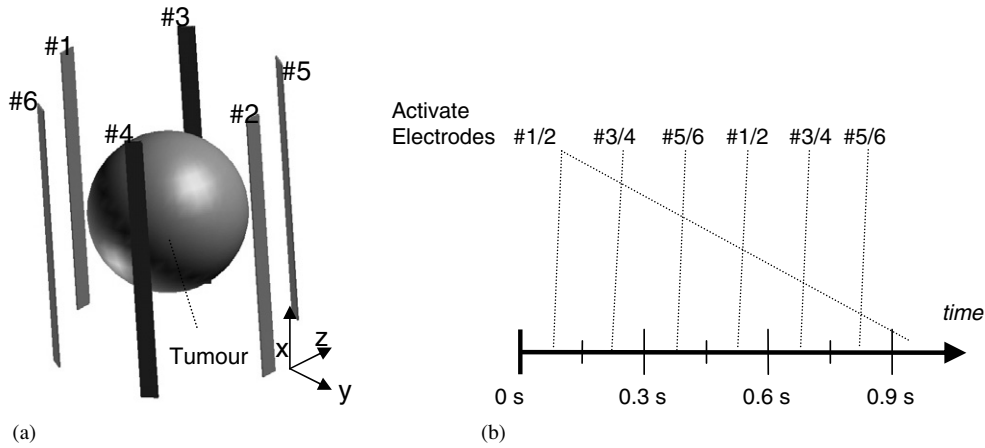


Figure 1. Illustration of the proposed structure with six electrodes (not to scale). All the electrodes have the dimensions $34 \text{ mm} \times 10 \text{ mm}$ and zero thickness. (a) Six electrodes (1–6) are placed surrounding a tumor. (b) Switching algorithm: RF energy is applied between opposing electrodes in a time sequential manner, between electrodes 1 and 2 for 100 ms, between electrodes 3 and 4 for 100 ms, etc.

The procedure is usually done in the frequency range of 400–600 kHz. For these frequencies, the wavelength in tissue is in the region of 500 m. Since the largest dimension of the structures of interest is much smaller than 1 m, it is possible to neglect any wave propagation effects and approximate the term $\mathbf{J} \cdot \mathbf{E}$ by $\sigma |\nabla V|^2$, where σ is the electrical conductivity (S m^{-1}) and V is the electric potential. We assume that σ is constant up to 100°C since the influence of its temperature dependence behavior is negligible in terms of ablation zone dimensions (Tungjtkusolmun *et al* 2000). In addition, it is possible to use the quasi-static approximation and obtain the electric potential V using a finite difference method for solving Laplace's equation (2) at the beginning of the simulation:

$$\nabla \cdot [\nabla V] = 0 \quad (2)$$

The FDM is used to solve all the partial derivatives involved in (1). Each derivative is approximated as shown in (3),

$$\begin{aligned} \frac{\partial \psi}{\partial t} &\approx \frac{\psi(s, t_2) - \psi(s, t_1)}{\Delta t} \\ \frac{\partial^2 \psi}{\partial s^2} &\approx \frac{\psi(s_2, t) - 2\psi(s, t) + \psi(s_1, t)}{\Delta s^2} \\ |\nabla V|^2 &\approx \left(\frac{V_2 - V_1}{\Delta s} \right)^2, \end{aligned} \quad (3)$$

where ψ is the temperature, t refers to the time and s refers to the spatial coordinates x , y and z .

The derivatives involved in (2) are calculated by similar approximations to those in (3). Here, an iterative algorithm for solving the equation is used. If, after two calculations, the difference between the previous and the current values for V is smaller than 0.001 V in the entire domain, the solution is reached. If not, V is recalculated for the entire domain. Since we apply voltages in the tens of volts range, this tolerance is suitable.

Table 1. Tissue electrical and thermal properties.

| | |
|--------------------------------------|--|
| Blood temperature (T_b) | 37 °C |
| Tissue density (ρ) | 1060 kg m ⁻³ |
| Electrical conductivity (σ) | 0.25 S m ⁻¹ |
| Thermal conductivity (k) | 0.502 W °C ⁻¹ m ⁻¹ |
| Tissue specific heat (c) | 3600 J kg ⁻¹ °C ⁻¹ |
| Blood density (ρ_b) | 1000 kg m ⁻³ |
| Blood specific heat (c_b) | 4180 J kg ⁻¹ °C ⁻¹ |
| Perfusion coefficient (ω) | 6.4 × 10 ⁻³ s ⁻¹ |

The computational domain of the simulation was 160 × 160 × 160 mm³. In the simulations, we used grid sizes of $\Delta s = 1$ mm and $\Delta t = 0.01$ s. The choice for Δt is not arbitrary, but it was selected to ensure the stability criterion, as in Incropera and DeWitt (1996). The choice for Δs was based on the desired accuracy. Larger values would result in faster simulations but at the expense of less accuracy. We tested $\Delta s = 1$ mm and $\Delta s = 0.5$ mm and the error between the two was less than 1% at the center of the domain. Dirichlet's boundary condition is used to truncate the computational domain. This means $V = 0$ and $T = 37$ °C (normal blood temperature) at the boundaries. The tissue parameters used in the simulations are given in table 1. In the simulations the electrodes were considered as plates with zero thickness and dimensions 34 mm × 10 mm.

In order to analyze the temperature profile for different electrode configurations, we simulated the circumferential configuration with different numbers of electrodes: four, six and eight electrodes. The actual shape for each configuration was rectangular, hexagonal and octagonal. For the simulations, we varied (a) the distance between the electrodes, (b) the voltage applied to the electrodes and observed the time required for the ablation procedure. Two stop criteria were used: the minimal temperature at any point at the center of the cylindrical volume defined by the electrode array and the total time for the procedure. Once the lowest temperature at the center of the volume reached 50 °C (typically considered the minimum temperature to cause cell death) or 90 °C (maximum temperature at the center when the electrodes reach 110 °C), the simulation would stop. Also, the simulation would cease if the procedure took more than 20 min in order to limit the ablation time to a clinically relevant period. In addition, we evaluated the switching time from 0.05 to 0.2 s in order to verify any influence of this parameter in the temperature profile. In order to calculate the dissipated power that results from a certain voltage one has to integrate the term $\mathbf{J} \cdot \mathbf{E} = \sigma |\nabla V|^2$ over the entire domain in equation (1). In clinical devices, maximum tissue temperature is limited to approximately 100–110 °C. Above 100 °C, tissue vaporization results in an electrically insulating region preventing further heating. Therefore, clinical devices use different control algorithms to keep maximum tissue temperatures close to 100 °C. Here, we used trial and error to determine the required voltage to produce tissue temperatures in the range of 100–110 °C. To simulate the behavior, we assumed the electric conductivity had the profile shown in equation (4). This prevents the simulation from producing excessively high temperature values:

$$\begin{aligned}
 \sigma(T) &= 0.25, & T < 100 \text{ °C} \\
 \sigma(T) &= 0.25 - (T - 100)/40, & 100 \text{ °C} < T < 110 \text{ °C} \\
 \sigma(T) &= 0, & T > 110 \text{ °C}.
 \end{aligned} \tag{4}$$

2.2. Experimental model

The results of the numerical simulations allowed us to guide the experimental study. In addition, the experimental study was used to validate the numerical model. Among the simulated configurations, we chose the one with a homogeneous temperature distribution while keeping a simple geometric configuration in order to build the experimental apparatus (6 electrodes, 1 cm wide, 4 cm electrode length, 4 cm separation). We performed an experimental trial. We used a piece of polyacrylamide gel (commonly used as a phantom for ablation studies) (Merkle *et al* 1999, McDonald *et al* 2004, McCann and Sherar 2006) with added bovine albumin to show coagulation. The electrical conductivity of the polyacrylamide gel was 0.25 S m^{-1} , its thermal conductivity was $0.56 \text{ W m}^{-1} \text{ K}^{-1}$ and its specific heat was $3810 \text{ J kg}^{-1} \text{ K}^{-1}$ (Davidson and Sherar 2003). The initial temperature of the phantom was $23 \text{ }^\circ\text{C}$ (room temperature) before the experiment was conducted. After the electrode array was inserted into the gel, a thermocouple array with three collinear sensing elements (IT-17(3), Physitemp, Clifton, NJ) was inserted at the center of the electrode array using a standard 16-gauge hypodermic needle. The three individual thermocouples were located 1 cm apart (see figure 9(a)). After placement of the electrodes and thermocouples, a custom control program and switching circuit was used to apply RF power from a commercial generator (500 W, 375 kHz, AEI PDX-500, Fort Collins, CO) sequentially to the electrode pairs with a switching period of approximately 150 ms for 5 min. Initially, we applied 100 V to the electrode pairs, and thereafter the voltage was automatically adjusted by the generator such that constant power (135 W) was applied to the electrodes. Since the computer model did not include temperature-dependent changes to electrical conductivity below $100 \text{ }^\circ\text{C}$, the computer model also applied constant power and thus the simulation and experimental results are comparable. We recorded the temperatures at the three thermocouples throughout the trial at a sampling rate of 100 Hz using a data acquisition card (DAQcard-6036E, National Instruments, Austin, TX) and then averaged the temperatures for comparison with the numerical simulation.

3. Results

3.1. Numerical simulation

For all simulations the interval between each switching was 0.1 s. Figure 2 shows the voltage distribution around the electrodes for the four-electrode configuration. The voltage distribution changes slightly for the six- and eight-electrode configurations. This was due to the presence of extra electric conductors, but it was concentrated around the plates that are turned on, as in the four-electrode configuration.

In figure 3, we changed the electrodes' voltage and observed the time necessary for the temperature at the center of our domain to reach $50 \text{ }^\circ\text{C}$ (i.e. to ablate the whole tissue region surrounded by the electrodes). As expected, the required voltage increased with electrode separation and a longer time was required to achieve $50 \text{ }^\circ\text{C}$ at the center. The maximum temperature was monitored and was $109.4 \text{ }^\circ\text{C}$ when we applied 110 V at 40 mm electrode distance.

In a second study, we used the configuration with six electrodes at the same distances as used in the four-electrode configuration. Figure 4 shows the time necessary to heat the center of the domain versus the applied voltage at the electrode. The maximum temperature was monitored and was $108.4 \text{ }^\circ\text{C}$ when we applied 110 V at 40 mm configuration.

In another analysis, we used a configuration with eight electrodes for the same distances as used in the two other configurations. The same exponential behavior was observed for the

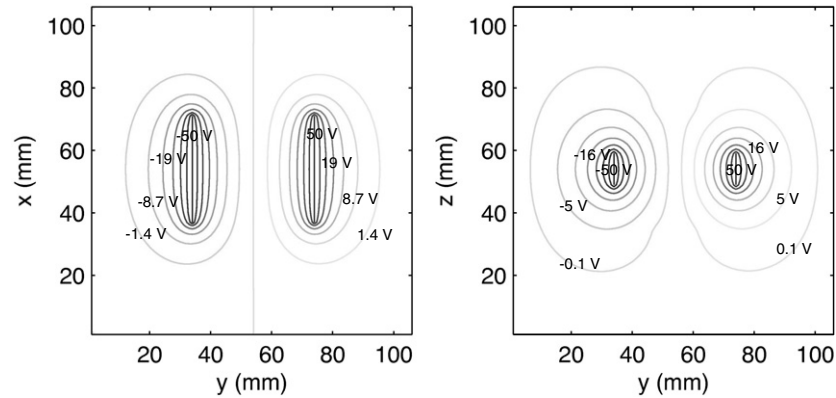


Figure 2. Voltage distribution around the electrodes for a four-electrode configuration in two different planes, at $z = 52$ mm and $x = 52$ mm, respectively. The voltage remains like this for 0.1 s, and then switches to the other pair (not shown).

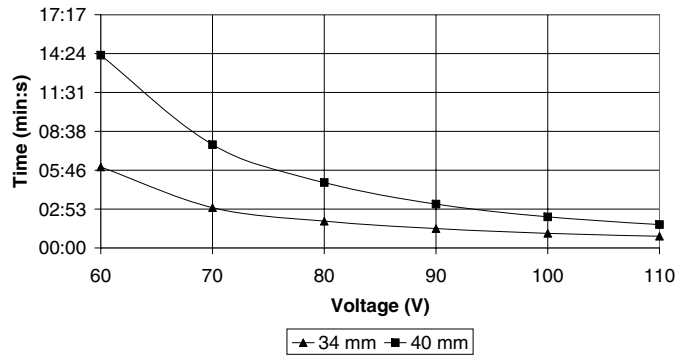


Figure 3. Time required to heat the center of the domain to 50 °C as a function of the voltage for a four-electrode configuration with a separation between opposite electrodes of 34 and 40 mm.

eight-electrode configuration when plotting the time to increase the temperature at the center to 50 °C as a function of the voltage for different distances between opposing electrodes. Figure 5 shows this behavior.

An additional investigation was to compare the performance of the three different configurations for the same voltage applied at the electrodes. Thus, we compared the time necessary to heat the center of our domain as a function of the distance between opposite electrodes for a fixed value of voltage (100 V). The results are shown in figure 6.

A very important analysis is to find the maximum possible voltage that does not result in considerable tissue charring, which creates an electrically insulated layer that prevents further power deposition into the liver tissue. We approximate the maximum possible voltage in the model by applying a voltage so that we have at least 90 °C at the center of the electrode. Figure 7 shows this behavior.

Furthermore, the temperature distribution that allows for estimating the ablation zone is significant. This is important since from that, we can determine the tumor size that can

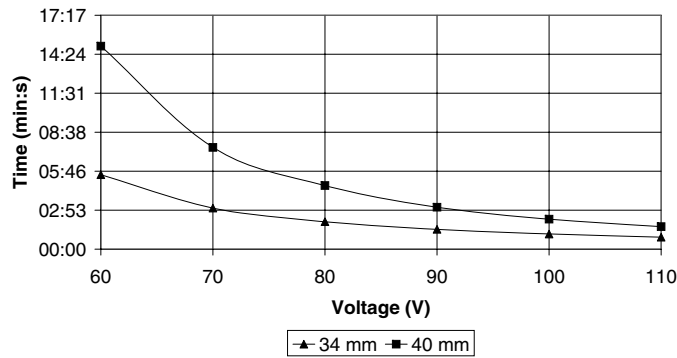


Figure 4. Time required to heat the center of the domain to 50 °C as a function of the voltage for a six-electrode configuration with a separation between opposite electrodes of 34 and 40 mm.

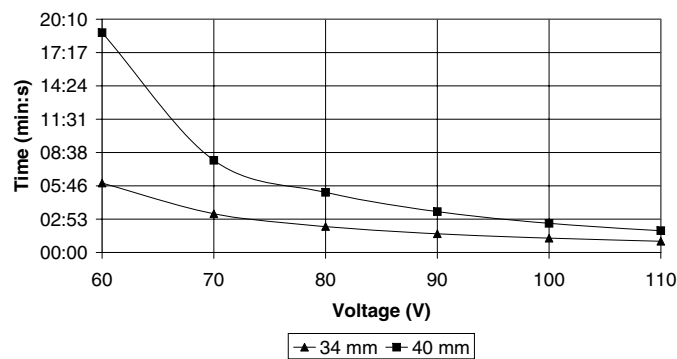


Figure 5. Time required to heat the center of the domain to 50 °C as a function of the voltage for an eight-electrode configuration with a separation between opposite electrodes of 34 and 40 mm.

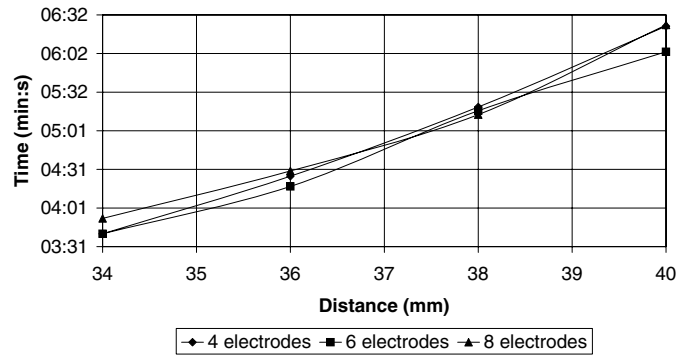


Figure 6. Time required to heat the electrode center to 90 °C for the four-, six- and eight-electrode configurations as a function of the distance between opposite electrodes for a fixed value of voltage (100 V).

potentially be treated with this device. We plotted the results for the three configurations. One can see the temperature profile for the three simulated configurations in figures 8(a)–(d).

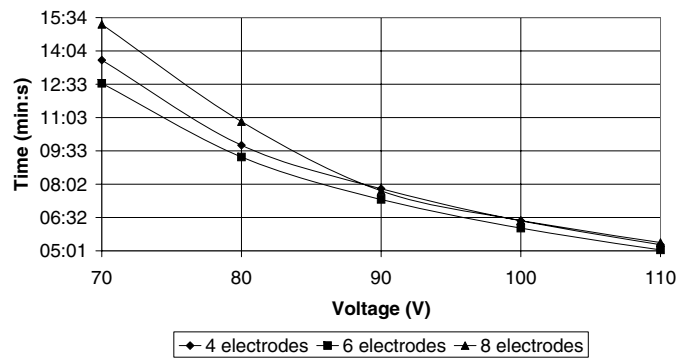


Figure 7. Time needed to heat the center of the volume to 90 °C for the four-, six- and eight-electrode configurations as a function of the voltage applied to the electrodes for a 40 mm separation between opposite electrodes.

An animated movie showing the evolution of the temperature with transparent planes can be seen at <http://www.ene.unb.br/~geb/heat.avi>.

3.2. Experiment

The extent of thermal coagulation during the experimental study can be seen in figures 9(a) and (b). Figures 9(c) and (d) show the results of the numerical simulation with the same parameters as in the experimental study. After 5 min, the final average temperature at the center of the array was 97 °C.

Figure 10 shows the temperature at the center of the phantom gel. As one can see, our model can accurately predict the temperature at the center of the phantom. The vertical bars show the standard deviation of the measured temperature at the surface of the phantom.

4. Discussion

Currently employed devices for tumor ablation typically use needle electrodes that are placed in the tumor, and subsequently heat the tumor from the center. While these devices generally work well for small tumors, treatment of large tumors is often time consuming and requires multiple ablations to treat the whole tumor.

In this study, we tested a new ablation device which employs multiple blade-shaped electrodes (figure 1(b)) that are inserted around the tumor for treatment of large tumors. This device is likely not feasible for use in minimally-invasive procedures, but would be simple to use during open surgery and possibly during laparoscopy. The multiple electrodes of the array are energized bipolar, where each pair of opposing electrodes is activated for brief time periods (figure 1(b)). We developed a three-dimensional finite difference code for analyzing three configurations with different numbers of electrodes (4, 6 and 8). Moreover, we performed an experimental *in vitro* study for validating the results. While our results demonstrated that larger volumes require longer procedures and higher voltages (see figures 6 and 7), we showed that ablation volumes up to 70 mm in diameter can be abated within less than 5 min. The comparison between figures 3 and 5 shows that increasing the number of electrodes from four to eight does not speed up the procedure considerably. This result is confirmed in figure 7. Moreover, figures 3–5 show that all the configurations take approximately the same time to

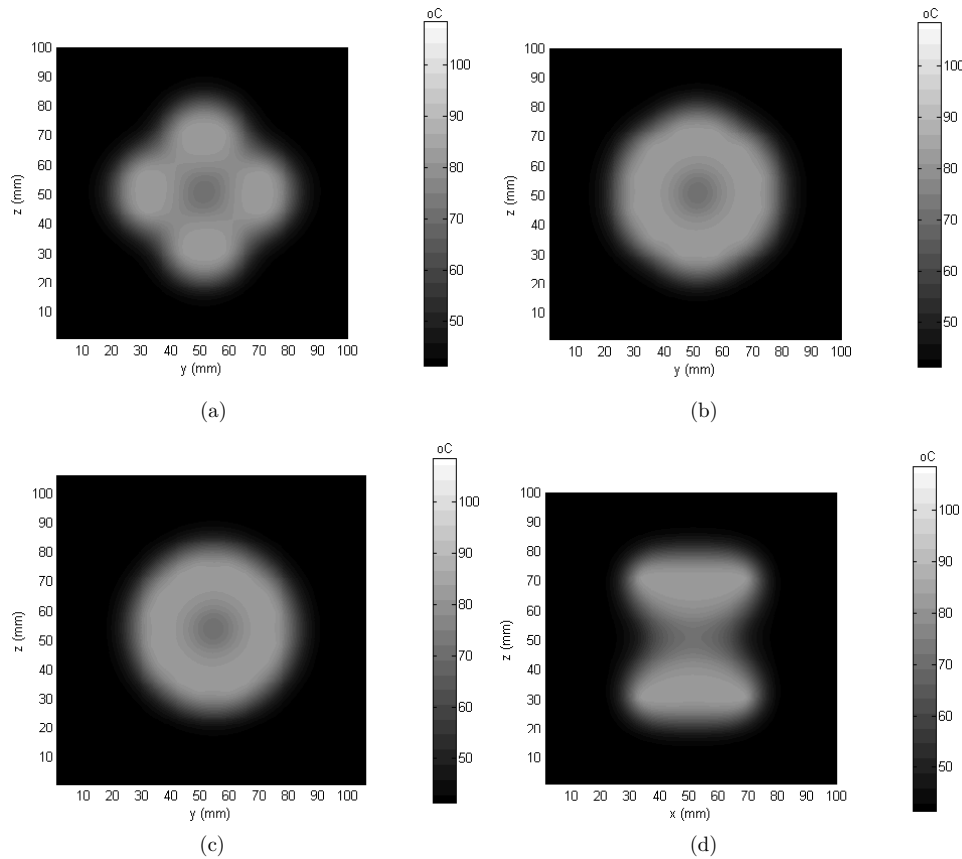


Figure 8. Temperature distribution for the three simulated configurations. We applied 100 V to the electrodes. The stop criterion is 90 °C at the center of the tumor. (a) The yz -plane for the four-electrode configuration. (b) The yz -plane for the six-electrode configuration. (c) The yz -plane for the eight-electrode configuration. (d) The xz -plane for the six-electrode configuration.

heat the center of the volume, suggesting little benefit of using large numbers of electrodes. Figures 3–5 show that if applied voltages (and therefore power) are sufficiently high (in our case, higher than 100 V), the ablation procedure takes nearly the same time for all the three configurations.

The results for simulations of the three configurations with faster and slower switching times (0.05 s and 0.2 s) did not show any difference, suggesting that a decrease in the switching time to less than 0.2 s is not beneficial. Since the switching time is much faster than the time-constant of tissue heating, from a heat-transfer point of view, all electrodes heat the tissue simultaneously.

Figures 8(a)–(d) and 9(a)–(d) show the size and geometry of the ablation zone that can be created with these devices. We found that we can ablate a cylindrical volume 70 mm in diameter and 40 mm high with six or eight electrodes placed 4 cm apart after 5 min ablation time due to thermal conduction from the electrodes radially outwards. The height of the ablation zone can potentially be adjusted in a patient-specific manner by varying the length of the active electrode region. Figures 8(a)–(c) show that in regard to the ablation zone geometry, the configurations

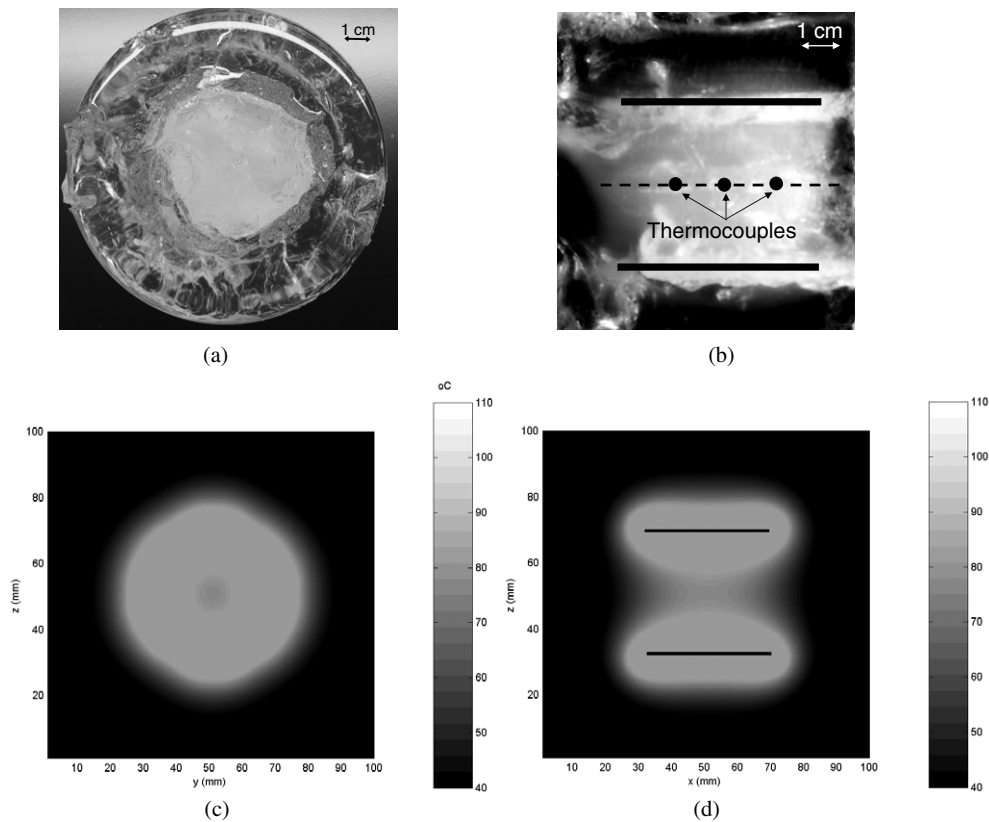


Figure 9. Representative ablation zones in gel phantoms (white regions are coagulated) and temperature profiles in the simulation. Solid lines mark electrode location. For the simulation, we used the thermal–electrical properties of the polyacrylamide gel, and perfusion was absent. (a) Top view of 4 cm array in gel phantom. (b) Center cross section of 4 cm array in gel phantom. (c) Top view of 4 cm array in simulation. (d) Center cross section of 4 cm array in simulation.

with six and eight electrodes perform better than the four-electrode configuration by creating a more spherical ablation zone.

Figure 8(d) illustrates that the temperature distribution and ablation zone shape in a plane parallel to the electrode axes assumes an hourglass shape.

Similar to standard tumor ablation devices, temperatures are the highest in close proximity of the electrodes. However, we do get a considerably more uniform temperature profile with the electrode array presented here with temperatures up to 90 °C at the center of the array, i.e. 2 cm from the electrodes. These higher temperatures would also suggest less susceptibility of the ablation zone to vascular mediated cooling by large vessels in proximity of the tumor.

One disadvantage of the proposed design is increased tissue trauma due to (1) insertion of multiple electrodes, and (2) larger (1 cm wide) electrodes in comparison to current devices, which may result in increased morbidity. We also note that there is heating and ablation of tissue outside the electrode array (see figure 9(d)). This is not necessarily a disadvantage since during ablation procedures the goal is to ablate the tumor plus a margin of 1 cm of surrounding normal tissue. That is, if the electrode array is placed right at the tumor boundary, ablation

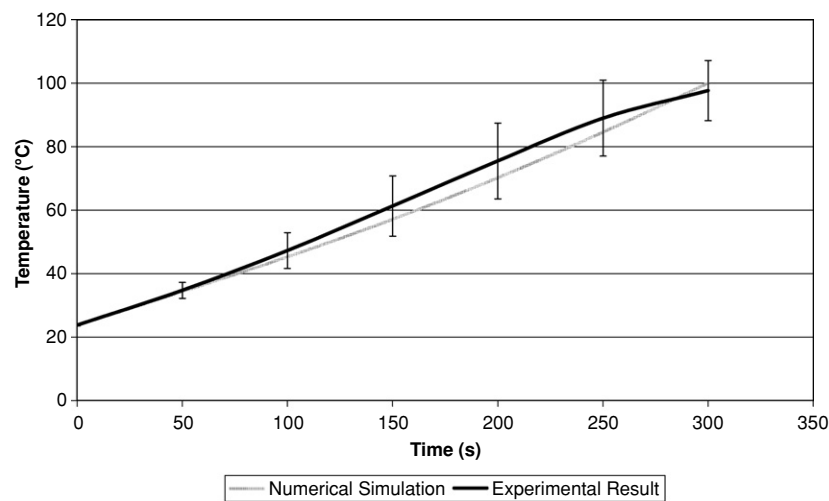


Figure 10. Comparison of simulated and experimental temperatures at the center of the ablated region versus time in a polyacrylamide gel phantom. For this computer simulation, properties of polyacrylamide gel were applied, and no perfusion was present.

outside the array may facilitate ablating the 1 cm rim of normal tissue. However, this issue has to be considered to avoid damage to nearby sensitive tissues (e.g. heart, diaphragm).

In addition to the computational models, we built a prototype device with six electrodes spaced 4 cm apart, and compared the temperature and size of the coagulated region to the computational models (figures 9(a)–(d) and 10). *In vitro* studies performed in a gel phantom confirmed that the volume within the electrodes can be coagulated (visualized in figures 9(a) and (b) as whitish regions) within 5 min. In addition, we found good correlation between temperatures measured in the phantom and in computational models (figure 10).

5. Conclusion

We presented a novel ablation device employing multiple blade-shaped electrodes. These allow more rapid heating of large volumes and provide more uniform tissue temperatures within the treatment region compared to current devices. Such a device may allow more effective treatment of large tumors during open surgery or laparoscopy.

Acknowledgments

This work was sponsored by the National Council for Scientific and Technological Development of Brazil (CNPq) under grants 301036/2006-3, 309430/2006-2 and 471489/2007-7, by the Coordination for the Improvement of Higher Education Personnel (CAPES) under grants 0263052 and 0013/08-0, and by Foundation of Support to Research for the Federal District (FAPDF) under grant 123/2007. Part of this work was conducted in a facility constructed with support from the National Institutes of Health, grant number C06 RR018823 from the Extramural Research Facilities Program of the National Center for Research Resources.

References

- Curley S A, Cusack J C, Tanabe K K, Stoelzing O and Ellis L M 2002 Advances in the treatment of liver tumors *Curr. Probl. Surgery* **39** 449–571
- Davidson S R and Sherar M D 2003 Measurement of the thermal conductivity of polyacrylamide tissue-equivalent material *Int. J. Hyperthermia* **19** 551–62
- Dodd G D, Frank M S, Aribandi M, Chopra S and Chintapalli K N 2001 Radiofrequency thermal ablation: computer analysis of the size of the thermal injury created by overlapping ablations *Am. J. Roentgenol.* **4** 777–82
- Gervais D A, McGovern F J, Arellano R S, McDougal W S and Mueller P R 2003 Renal cell carcinoma: clinical experience and technical success with radio-frequency ablation of 42 tumors *Radiology* **226** 417–24
- Gillams A R 2005 The use of radiofrequency in cancer *Br. J. Cancer* **92** 1825–9
- Groenemeyer D H, Schirp S and Gevargez A 2002 Image-guided percutaneous thermal ablation of bone tumors *Acad. Radiol.* **9** 467–77
- Haemmerich D, Schutt D J, Will J A, Striegel R M, Webster J G and Mahvi D M 2004 A device for radiofrequency assisted hepatic resection *Conf. Proc. IEEE Eng. Med. Biol. Soc.* vol 4 pp 2503–6
- Incropera F P and DeWitt D P 1996 *Fundamentals of Heat and Mass Transfer* 4th edn (New York: Wiley)
- Lee F T Jr, Haemmerich D, Wright A S, Mahvi D M, Sampson L A and Webster J G 2003 Multiple probe radiofrequency ablation: pilot study in an animal model *J. Vasc. Interv. Radiol.* **14** 1437–42
- Mayo-Smith W W and Dupuy D E 2004 Adrenal neoplasms: Ct-guided radiofrequency ablation—preliminary results *Radiology* **231** 225–30
- McCann C and Sherar M D 2006 Development of a novel loosely wound helical coil for interstitial radiofrequency thermal therapy *Phys. Med. Biol.* **51** 3835–50
- McDonald M, Lochhead S, Chopra R and Bronskill M J 2004 Multi-modality tissue-mimicking phantom for thermal therapy *Phys. Med. Biol.* **49** 2767–78
- Merkle E M, Goldberg S N, Boll D T, Shankaranarayanan A, Boaz T, Jacobs G H, Wendt M and Lewin J S 1999 Effects of superparamagnetic iron oxide on radio-frequency-induced temperature distribution: in vitro measurements in polyacrylamide phantoms and in vivo results in a rabbit liver model *Radiology* **212** 459–66
- Neeman Z and Wood B J 2002 Radiofrequency ablation beyond the liver *Tech. Vasc. Interv. Radiol.* **5** 156–63
- Nguyen C L, Scott W J, Young N A, Rader T, Giles L R and Goldberg M 2005 Radiofrequency ablation of primary lung cancer: results from an ablate and resect pilot study *Chest* **128** 3507–11
- Ni Y, Miao Y, Michel L and Marchal G 2005 A review of the general aspects of radiofrequency ablation *Abdom. Imaging* **30** 381–400
- Pennes H H 1948 Analysis of tissue and arterial blood temperature in the resting human forearm *J. Appl. Physiol.* **1** 93–122
- Schutt D J, O'Rourke A P, Will J A, Webster J G, Mahvi D M and Haemmerich D 2008 An electrode array that minimizes blood loss for radiofrequency-assisted hepatic resection *Med. Eng. Phys.* **30** 454–9
- Tungjitkusolmun S, Whoo E J, Cao H, Tsai J Z, Vorperian V R and Webster J G 2000 Thermal-electrical finite element modelling for radio frequency cardiac ablation: effects of changes in myocardial properties *Med. Biol. Eng. Comput.* **38** 562–8